Korean J. Chem. Eng., 36(10), 1669-1679 (2019)
DOI: 10.1007/s11814-019-0351-6

pISSN: 0256-1115
eISSN: 1975-7220

An experiment and model of ceramic (alumina) hollow fiber membrane contactors for chemical absorption of CO_2 in aqueous monoethanolamine (MEA) solutions

Hong Joo Lee, Michael Binns, Sang Jin Park, Edoardo Magnone, and Jung Hoon Park†

Dongguk University, Wonheung-gwan F619, 30, Pildong-ro 1gil, Jung-gu, Seoul 04620, Korea
(*Received 12 May 2019 • accepted 5 August 2019*)

Abstract−The chemical absorption of CO_2 in a monoethanolamine (MEA) solution by a ceramic hollow fiber membrane contactor (HFMC) was investigated experimentally and numerically to obtain the best compromise between the mass transfer coefficient and structural characteristics such as membrane pore size and porosity. The mathematical model derived is based on the three resistances in the resistance-in-series model. The accuracy of the numerical simulation was verified quantitatively by the experimental data obtained in this study. A good agreement between experimental and computational results was found with an average absolute deviation (AAD) between observed data and predicted values of 2.86%. In addition, the effects of the operating condition (i.e., gas and liquid flow rates) on the mass transfer coefficients for ceramic HFMC systems were also studied, revealing that the membrane and gas-phase mass transfer resistances were dominant factors in the overall mass transfer. In conclusion, the present study suggests that the membrane structure plays a very important role in the optimization of HFMC performance. In fact, the best results were obtained with an intermediate range of the pore size between 10^2 and 10^4 nm, corresponding to the best compromise between performance (i.e., overall mass transfer coefficient) and applicability (i.e., breakthrough pressure).

Keywords: Membrane Contactor, Hollow Fiber Membrane, Ceramic Membrane, CO_2 Absorption, Modeling

INTRODUCTION

Carbon dioxide (CO_2) is considered as the most important exhaust gas, and it potentially plays an important role in the acceleration of global warming. Recently, considerable research attention has focused on the capture of CO_2 from a stationary source with CO_2 Capture and Storage (CCS) technology [1]. Particularly, the separation of CO_2 and N_2 from flue gases is very important in the post-combustion CO_2 capture process because ambient air is commonly used for fuel combustion. The different methods of CO_2 capture include the absorption column on chemical and physical solvent, which is a well-known industrial process [2]. However, CO_2 capture with a conventional absorption process requires large equipment and high energy. Hence, it is profitable to develop new technology for CO_2 capture with lower costs [3]. There is an increasing interest in the use of membrane contactors for CO_2 capture from power-plant flue gas. A gas-liquid hollow fiber membrane contactor (HFMC) process for gas separation has important advantages when compared with conventional absorption processes such as increased interfacial area, increases in the capacity factor, and lower energy consumption [4].

Thus, several researchers have studied polymeric HFMC for CO_2 capture [5-11]. However, there are limitations in applying polymeric membranes for the membrane contactor process due to low chemical and thermal stability properties. Performance degradation of the polymeric HFMC has been reported due to pore swelling by the absorbent [12]. In contrast, ceramic materials have little reactivity with a chemical solvent. To enhance operation stability of the HFMC system, several authors studied the feasibility of porous ceramic HFMC and presented comprehensive experimental reports [13-15]. Although ceramic membrane production cost is typically higher than the polymeric membrane production cost, research has examined ceramic HFMC for durability and performance improvement. A recent study involved an experimental analysis of the possible laboratory-scale applications of a modified hydrophobic aluminum oxide hollow fiber membrane for physical absorption of CO_2 into H_2O [13]. Koonaphapdeelert et al. tested an HFMC stripping process with a porous alumina membrane and verified that the porous alumina membrane could improve the CO_2 absorption properties and process durability when compared with traditional polymeric membranes for HFMC applications [14]. In addition, the long-term stability of the ceramic HFMC was experimentally confirmed in our previous study [15]. There was a slight performance decrease after 70 hours of operation, but no pore swelling or loss of hydrophobic coating layer was observed. [15].

It is very important to improve and optimize the HFMC process as well as the material of the membrane to enhance the stability and performance of the process. Specifically, numerical modeling of the HFMC for CO_2 capture application is a foundational and crucial point to improve the fundamental understanding of HFMC and then obtaining an optimal compromise between the system variables in terms not only of membrane pore size but also of porosity and performance. Furthermore, the process model can be used as a fundamental tool to build a computer simulation platform in the field economic evaluation studies. Thus, a large number of existing studies in the broader literature have examined the HFMC modeling. Ozturk et al. [5] studied mass transfer characteristics of silicone rubber and polypropylene (PP) HFMC for CO_2 removal by numeri-

†To whom correspondence should be addressed.
E-mail: pjhoon@dongguk.edu

cal simulation and experiments. Boributh et al. [6] developed a mathematical model for polyvinylidenefluoride (PVDF) HFMC and validated the same with experimental results. Hashemifard et al. [7] performed a numerical simulation to evaluate partial pore wetting and discussed mass transfer in polyetherimide (PEI) and polyethersulfone (PES) HFMC. The literature review shows that several previous investigations examined the modeling of the polymeric HFMC. In contrast, to the best of our knowledge, there is no previously published work that directly investigates the modeling and optimization of structural parameters of the ceramic HFMC system for the chemical absorption of CO_2.

From a modeling viewpoint, the main purpose of this study was to examine the ceramic HFMC performance for CO_2 separation. The modeling of the chemical absorption of CO_2 into an aqueous monoethanolamine (MEA) solution using porous alumina HFMC was performed by a numerical method derived from a resistance-in-series model approach where the overall mass transfer coefficient is a combination of three different factors like mass transfer coefficients of gas, membrane, and liquid phase. Subsequently, the investigated model for ceramic HFMC was validated by quantitatively comparing the simulated overall mass transfer coefficient data with experimental data in a gas velocity range between 1.5×10^{-4} m/s and 9×10^{-4} m/s. In addition, this study also examined the relationship between the CO_2 concentration (5-30% CO_2) as well as the liquid velocity (0.3×10^{-3}-5×10^{-3} m/s) on the CO_2 absorption properties of the HFMC system for chemical absorption of CO_2 into the aqueous monoethanolamine (MEA) solution. As far as we know, no previous research has investigated the role of individual mass transfer coefficient contributions on the overall mass transfer coefficient in the case of the ceramic HFMC by a numerical model validated through comparison with experimental data.

Furthermore, there are key questions that are still not completely discussed in the literature. In this context, "what morphological conditions are suitable to obtain a high performance (i.e., high overall mass transfer coefficient) as well as high stability (i.e., high breakthrough pressure) for a ceramic HFMC?" is arguably an important question to be addressed. To the best of our knowledge, this question has never been addressed in depth in case of the ceramic HFMCs for chemical absorption of CO_2 in aqueous monoethanolamine (MEA) solutions. For example, Li et al. [8] studied pore structure effects on the mass transfer coefficients of a polymeric membrane as PVDF from both theoretical and practical viewpoints. The analysis indicated that a high mass transfer coefficient of a membrane could be achieved with a large pore size and high porosity, although significant effects on the performance were not observed at a pore radius that exceeded approximately 10^3 nm [8]. Atchariyawut et al. [9] investigated the influence of the structure of polymeric membranes, such as microporous PVDF hollow fibers, on the mass transfer. Specifically, the authors demonstrated that the contribution of membrane resistance to the overall mass transfer resistance followed a resistance-in-series model approach in which the overall mass transfer increased with decreases in the molecular weight cut-off (MWCO) and the finger-like pores [9]. Finally, Bakeri et al. [10] observed a strong correlation between CO_2 absorption property, pore size, and porosity of the surface-modified polyetherimide hollow fiber membrane in which the CO_2 absorption value increased with increases in the pore size of the polymeric membrane. Interestingly, Korminouri et al. [11] suggested an inverse relationship between breakthrough pressure and membrane pore size in a polysulfone (PSf) HFMC. However, modeling studies exclusively focused on polymeric membranes [8-11] and there is a paucity of studies examining the modeling and optimization of ceramic HFMC for the chemical absorption of CO_2 into MEA solutions. The model parameters in polymeric HFMC are well known in previous reports [8-11]. However, to the best of our knowledge, no model parameters of ceramic HFMC process have been reported.

Hence, to overcome the afore-mentioned gap between polymeric and ceramic HFMCs and to simultaneously increase knowledge and understanding of ceramic HFMCs for practical application, the main objectives of the present study included the following: (1) Examining a simulation model to identify and evaluate optimal parameters (e.g., gas or liquid velocity and CO_2 concentration) to improve the performance of ceramic HFMC, (2) performing a detailed analysis of correlations between mass transfer coefficient and structural characteristics (e.g., membrane pore size and porosity) of ceramic HFMC, and (3) proposing general guidelines to determine fundamental specifications and to develop a strategy for the overall CO_2 capture process.

EXPERIMENTS AND MODELS

1. Experimental Procedures

The preparation of porous Al_2O_3 hollow fiber membrane is based on the phase inversion technique followed by the sintering process at high temperatures. The formation of a depth finger-like structure is usually attributed to the nature of a fast interaction between the spinning suspension - consisting of Al_2O_3 powder, polymer binder, and solvent - and a non-solvent positioned on the precipitation bath. At the same time, during spinning, an internal precipitant is continuously provided through the central tube of a tube-in-orifice spinneret. In general, it can be expected that, during the phase inversion process, the pore structure of final Al_2O_3 hollow fiber membrane can be controlled by ratio between the components of spinning suspension, nature of solvent and non-solvent type, extrusion rate of the spinning suspension, internal coagulant flow rate, air gap between spinneret and external precipitation bath, and so on [13].

In this work, Al_2O_3 powder, 1-methyl-2-pyrrolidone (NMP, 99.5%, Samchun Pure Chemical Co., Ltd., Korea), polyethersulfone (PESf, Ultrason® E6020P, BASF, Germany), and polyvinylpyrrolidone (PVP, Sigma-Aldrich, U.S.A.) were used for preparing a spinning suspension. The suspension was mixed for 48 hours. The suspension was mixed for 48 hours and then the iron tank containing the prepared suspension was pressurized by an inert gas for the spinning process. The spinning suspension was extruded through a spinneret nozzle and, at the same time, a coagulant was fed into the nozzle. A water bath at room temperature (23 °C) was utilized for the phase inversion process. The obtained green bodies were dried and finally sintered at 120 °C and 1,300 °C, respectively. A mercury porosimeter (AutoPore IV 9500, Micromeritics Instruments Corp., U.S.A.) was used to measure the membrane pore size and porosity. The membranes were coated with heptadecafluoro-1,1,2,2-

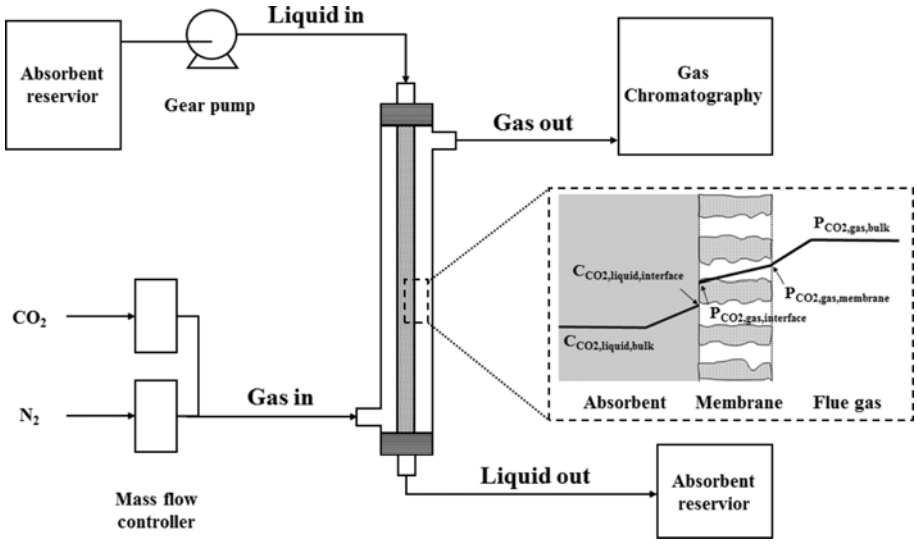

Fig. 1. A diagram of the absorption HFMC used in the experiment section and details of the mass transfer mechanism.

tetrahydrodecyltrimethoxysilane (FAS, >98%, Sooyang Chemtex Co., Ltd., Korea) to convert the nature of the surface of the membrane from hydrophilic to hydrophobic. As shown in the scheme depicted in Fig. 1, CO_2 absorption tests were performed for hydrophobic modified porous alumina HFMC with a monoethanolamine (MEA) solution. The lab-scale module consisted of single Al_2O_3 hollow fiber membranes with a length of 150 mm. Additionally, gas chromatography (GC-TCD, Master GC, Dani, Italy) was used in the system to measure the CO_2 concentration in the outlet of the gas stream. The operation was performed at atmospheric pressure and room temperature. The experimental configuration consisted of a simulated flue gas flow (CO_2 15% and N_2 balanced) and an absorbent (MEA) flow. Further details are reported elsewhere [13].

2. Modeling of the Overall Mass Transfer Coefficient (K_L) in HFMC

The local flux of the CO_2 gas transfer through the membrane at steady state can be expressed as follows [14]:

$$J_{CO_2} = K_L(C_{CO_2} - C^*_{CO_2}) \quad (1)$$

where J_{CO_2} is the mass transfer flux (mol/m^2·s^{-1}), and K_L is the overall mass transfer coefficient (m/s). C_{CO_2}, and $C^*_{CO_2}$ is the CO_2 concentrations in the solvent, and equilibrium CO_2 concentration of the solvent (mol/m^2), respectively.

Fig. 1 shows the mass transfer mechanism in the case of HFMC by a resistance-in-series model approach. As clearly shown, the overall process can be considered as occurring through three resistances in serie: gas, membrane, and liquid phase resistances. Therefore, the overall mass transfer coefficient (K_L) for the non-wetted membranes can be expressed by a resistance-in-series model approach as follows [14]:

$$\frac{1}{K_L} = \frac{1}{Hk_g} + \frac{1}{Hk_m} + \frac{1}{Ek_l} \quad (2)$$

where k_g, k_m, and k_l are the individual mass transfer coefficients of gas, membrane, and liquid phase, respectively. H corresponds to the Henry's law constant of CO_2 in the absorbent and E is the enhancement factor. The following assumptions were used for the mathematical model proposed in this study: The HFMC system (1) works in an isothermal condition and (2) in the steady-state continuous flow mode. In addition, it is supposed that (3) the natural gas follows the ideal gas law, (4) liquid flows on the lumen side of the fiber, and (5) gas flows on the shell side of the fiber. The method used to calculate the contributions of the individual mass transfer coefficient (k_l, k_m, and k_g) to the overall mass transfer coefficient (K_L) is discussed in the next section.

2-1. Liquid Phase Mass Transfer Coefficient (k_l)

When the solvent was flying in the lumen side in the hollow fiber membrane, the liquid phase mass transfer coefficient (k_l) could be determined by Leveque correlation [16] as follows:

$$Sh = 3.67, \ Gz < 10 \quad (3)$$

$$Sh = 1.615(Gz)^{1/3}, \ Gz > 20 \quad (4)$$

where the Sherwood (Sh) and Graetz (Gz) numbers can be calculated by the following formulas:

$$Sh = k_l d_i / D_{CO_2, MEA} \quad (5)$$

and

$$Gz = d_i^2 v_l / D_{CO_2, MEA} \, L \quad (6)$$

Kreulen et al. [17] suggested an available correlation equation irrespective of the Graetz (Gz) number. Thus, the liquid phase mass transfer coefficient (k_l) could be calculated with this correlation as follows:

$$Sh = \sqrt[3]{(3.67)^3 + (1.615)^3 Gz} \quad (7)$$

$$k_l = \frac{D_{CO_2, MEA}}{d_i}\left((3.67)^3 + (1.615)^3\left(\frac{d_i^2 v_i}{D_{CO_2, MEA} \, L}\right)\right) \quad (8)$$

where $D_{CO_2, MEA}$, v_i, L and d_i are the diffusion coefficient of CO_2 in the MEA solution (m^2/s), liquid velocity (m/s), fiber length (m),

and fiber inner diameter (m), respectively. Specifically, the diffusion coefficient of CO_2 in the MEA solution was calculated using an analogy with N_2O, where the correlation between the diffusion coefficients of CO_2 ($D_{CO_2, MEA}$) and N_2O ($D_{N_2O, MEA}$) in a MEA solution [18] is represented by the following equation:

$$D_{CO_2, MEA} = D_{N_2O, MEA} \frac{D_{CO_2, H_2O}}{D_{N_2O, H_2O}} \tag{9}$$

The diffusivity of CO_2 (D_{CO_2, H_2O}) and N_2O (D_{N_2O, H_2O}) in water could be calculated by two temperature-dependent functions as follows [18]:

$$D_{CO_2, H_2O} = 2.35 \times 10^{-6} \exp\left(\frac{-2119}{T}\right) \tag{10}$$

$$D_{N_2O, H_2O} = 5.07 \times 10^{-6} \exp\left(\frac{-2371}{T}\right) \tag{11}$$

where T is the temperature in Kelvin (K). Additionally, Ko et al. [19] suggested a mathematical correlation between the diffusivity of N_2O in a MEA solution ($D_{N_2O, MEA}$) expressed in m^2/s and the MEA concentration in solution. This relation is expressed by the following equation:

$$D_{N_2O, MEA} = (5.07 \times 10^{-6} + 8.65 \times 10^{-7} C_{MEA} + 2.78 \times 10^{-7} C_{MEA}^2) \times \exp\left(\frac{-2371 - 93.4 C_{MEA}}{T}\right) \tag{12}$$

where C_{MEA} is the molarity of MEA solution (mol/m^3). Hence, based on Eq. (9), it is possible to calculate the $D_{CO_2, MEA}$.

2-2. Membrane Phase Mass Transfer Coefficient (k_m)

As reported by previous studies [8], the membrane phase mass transfer coefficient (k_m) could be expressed as follows:

$$k_m = \frac{D_{CO_2, m} \varepsilon}{\delta \tau_m} \tag{13}$$

where $D_{CO_2, m}$ is the effective membrane diffusion coefficient (m^2/s), ε is the membrane porosity, δ is membrane thickness (m) and τ_m is tortuosity. A tortuosity of 2.5 was used in the calculation of the mass transfer coefficient, since values of 2-3 were reported in previous studies [20] and [21]. Table 1 shows the experimental parameters of the HFMC module for the study.

The diffusion process through the membrane is governed by two coefficients, the bulk and the Knudsen diffusion [22]. The mathematical relationship between these two coefficients is presented by by the following formula:

$$\frac{1}{D_{CO_2, m}} = \frac{1}{D_{CO_2, gas}} + \frac{1}{D_{Kn}} \tag{14}$$

where $D_{CO_2, gas}$ and D_{Kn} denote the bulk diffusion coefficient and the Knudsen diffusion coefficient, respectively. Both types of diffusion can coexist with an average pore size (d_p) between 10^2 nm and 10^4 nm [22]. The region with an average pore size between 10^2 nm and 10^4 nm is termed as a transition region. Regions with average pore sizes below 10^2 nm and above 10^4 nm as Knudsen and bulk diffusion dominant regions, respectively.

The bulk diffusivity of CO_2 ($D_{CO_2, gas}$) in a gas mixture (CO_2 and N_2) can be calculated by the Chapman-Enskog equation as follows [23]:

$$D_{CO_2, gas} = \frac{0.001858 T^{3/2} [(M_{CO_2} + M_{N_2})/M_{CO_2} M_{N_2}]^{1/2}}{P \sigma_{CO_2, N_2}^2 \Omega_D} \tag{15}$$

where M_{CO_2} and M_{N_2} denote molecular weight of CO_2 and N_2, respectively. P is the pressure (Pa), σ_{CO_2, N_2} is the arithmetic mean characteristic length (Å) of CO_2 and N_2, and Ω_D is the diffusion collision integral. It is useful to note that the denominator (σ_{CO_2, N_2}) in Eq. (15) can be estimated as follows:

$$\sigma_{CO_2, N_2} = \frac{\sigma_{CO_2} + \sigma_{N_2}}{2} \tag{16}$$

where σ_{CO_2} (=3.941) and σ_{N_2} (=3.798) represent the characteristic length of CO_2 and N_2, respectively. Furthermore, the diffusion collision integral (Ω_D) (as shown in Eq. (15)) is a function of temperature and can be expressed as follows [23]:

$$\Omega_D = \frac{a_1}{(T^*)^{a_2}} + \frac{a_3}{\exp(a_4 T^*)} + \frac{a_5}{\exp(a_6 T^*)} + \frac{a_7}{\exp(a_8 T^*)} \tag{17}$$

where a_1 (=1.06036), a_2 (=0.15610), a_3 (=0.19300), a_4 (=0.47635), a_5 (=1.03587), a_6 (=1.52996), a_7 (=1.76474), and a_8 (=3.89411) denote constants. Thus, the value of the dimensionless temperature T^* (see Eq. (17)) can be calculated as follows:

$$T^* = \frac{BT}{\varepsilon_{CO_2, N_2}} \tag{18}$$

where B is Boltzmann's constant and ε_{CO_2, N_2} is the characteristic energy determined as follows:

$$\varepsilon_{CO_2, N_2} = (\varepsilon_{CO_2} \times \varepsilon_{N_2})^{1/2} \tag{19}$$

where ε_{CO_2} and ε_{N_2} are the characteristic energies of CO_2 (ε_{CO_2}/B= 195.2 K) and N_2 (ε_{N_2}/B=71.4 K), respectively.

Knudsen diffusion coefficient (D_{Kn}) in the Eq. (14) can be calculated by the following equation [22]:

$$D_{Kn} = \frac{2 r_p}{3} \sqrt{\frac{8RT}{\pi M_{CO_2}}} \tag{20}$$

where r_p is the membrane pore radius (m) and M_{CO_2} is the molecular weight of CO_2 (as shown in Eq. (15)).

2-3. Gas Phase Mass Transfer Coefficient (k_g)

As shown in Table 2, several experimental and analytical stud-

Table 1. Properties of the HFMC module

Parameter	Value	Unit
Fiber inner diameter	1.44×10^{-3}	m
Fiber outer diameter	2.22×10^{-3}	m
Effective length	1.50×10^{-1}	m
Module inner diameter	7.53×10^{-3}	m
Pore size	3.091×10^{2}	nm
Porosity	54.27	%
Tortuosity	2.5	-
Temperature	20	°C
Pressure	Atmospheric pressure	-

Table 2. Shell side mass transfer correlations

Correlations	Reynolds number	Packing factor	Reference
$Sh=1.25\left(Re\frac{d_e}{L}\right)^{0.93}Sc^{0.33}$	0.5<Re<500	Ø=0.03	M. C. Yang [24]
$Sh=1.38Re^{0.34}Sc^{0.33}$	1<Re<25	Ø=0.7, single fiber	M. C. Yang [24]
$Sh=0.90Re^{0.40}Sc^{0.33}$	1<Re<25	Ø=0.07, single fiber	M. C. Yang [24]
$Sh=(0.53-0.58Ø)Re^{0.53}Sc^{0.33}$	21<Re<324	0.32<Ø<0.76	M. J. Costello [25]
$Sh=0.61Re^{0.363}Sc^{0.333}$	0.6<Re<49	Ø=0.003	P. Cotel [26]
$Sh=5.8(1-Ø)\left(\frac{d_e}{L}\right)Re^{0.6}Sc^{0.3}$	0<Re<500	0.04<Ø<0.4, hydrophobic	R. Prasad [27]
$Sh=6.1(1-Ø)\left(\frac{d_e}{L}\right)Re^{0.6}Sc^{0.3}$	0<Re<500	0.04<Ø<0.4, hydrophilic	R. Prasad [27]

ies focused on the shell side mass transfer of HFMC. Consequently, the empirical mathematical correlation between all system variables could be derived directly based on extant research as follows:

$$Sh=f(Ø)\times\left(\frac{d_e}{L}\right)^{\alpha}\times Re^{\beta}\times Sc^{\gamma} \tag{21}$$

where Ø is the packing density and d_e is the hydraulic diameter calculated, in turn, as 4A/U, where A is the cross section area of the module while U is the module wetted perimeter that corresponds to the sum of internal module perimeter and the total perimeter of all hollow fibers. α, β, and γ are constants. Re is the Reynolds number ($Re=d_e\rho v_g/\mu$), and Sc is Schmidt number ($Sc=\mu/\rho D_{CO_2,gas}$). ρ and μ [23] are the gas density and viscosity, respectively.

For a given membrane module, Ø, d_e, and L are constant and well known. In all the cases reported in Table 2, γ value corresponds always to 0.33, and thus Eq. (21) could be simplified as follows:

$$Sh=a\times Re^{b}\times Sc^{0.33} \tag{22}$$

According to Table 2, the a and b parameters are functions of other experimental parameters. In fact, these two parameters are linked in turn to the structural characteristics and geometry of membrane as well as type of membrane module and operating conditions. These parameters can be calculated and applied in a polymeric HFMC because, as introduced, there have been numerous studies to investigate the polymeric systems [24-27]. However, to the best of our knowledge, there are no studies that examine ceramic HFMC from the present point of view and in the sense of the a and b parameters. It would be of special interest to enhance these studies in terms of ceramic HFMC. Therefore, one of the objectives of this work was to determine the optimum (a, b) parameters for maximizing not only the performance but also the applicability of the ceramic HFMC.

2-4. Enhancement Factor (E)

DeCoursy et al. [28] suggested an approximation method for estimating the enhancement factor (E) reported in Eq. (2) as follows:

$$E=\frac{-Ha^2}{2(E_\infty-1)^2}+\sqrt{\frac{Ha^4}{4(E_\infty-1)^2}+\frac{E_\infty Ha^2}{(E_\infty-1)}+1} \tag{23}$$

where Ha and E_∞ are the Hatta number and the infinite enhancement factor, respectively. Specifically, Hatta number can be defined as follows:

$$Ha=\frac{\sqrt{D_{CO_2,MEA}C_{MEA}k}}{k_l} \tag{24}$$

where k (m^3/mol·s) is the rate constant of the reaction between CO_2 and MEA reaction [29] and can be expressed as follows:

$$\log k=10.99-2152/T \tag{25}$$

$$E_\infty=\left(1+\frac{C_{MEA}D_{MEA}}{v_R C_{CO_2,I}D_{CO_2,MEA}}\right)\left(\frac{D_{CO_2,MEA}}{D_{MEA}}\right) \tag{26}$$

where v_R is the stoichiometric coefficient of the overall reaction, and D_{MEA} is the MEA diffusivity in an aqueous MEA solution. Additionally, D_{MEA} can be determined as follows [30]:

$$D_{MEA}=\exp(-13.275-2198.3/T-7.8142\times10^{-5}C_{MEA}) \tag{27}$$

where $C_{CO_2,I}$ can be determined by a mathematical expression already previously proposed by Khaisri et al. [29] in the following way:

$$C_{CO_2,I}=\left(\frac{p_{CO_2,g}+(k_l(d_i/d_o)E/k_g')C_{CO_2,MEA}}{1+(k_l(d_i/d_o)E/Hk_g')}\right)H \tag{28}$$

where $p_{CO_2,g}$ and $C_{CO_2,MEA}$ are the partial pressure of the CO_2 in the gas phase and the CO_2 concentration in a MEA solution, respectively, and k_g' is determined by the following expression [29]:

$$k_g'=\frac{k_g/RT}{1+(k_g/k_m)(d_o/d_m)} \tag{29}$$

where d_o and d_m are hollow fiber outer and log mean diameters, respectively.

2-5. Henry's Constant (H)

In the case in the present study, Henry's law constant (H) of CO_2 in MEA solution can be calculated from Henry's law constant of N_2O by using the following equation [32]:

$$H=H_{CO_2,MEA\text{-}sol}=H_{N_2O,MEA\text{-}sol}\frac{H_{CO_2,H_2O}}{H_{N_2O,H_2O}} \tag{30}$$

Henry's law constants of N_2O (H_{N_2O,H_2O}) and CO_2 (H_{CO_2,H_2O}) in water as a function of temperature (T) are reported as follows:

$$H_{N_2O,\,H_2O}=\exp\left(158.245-\frac{9048.596}{T}-20.860\ln T-0.00252T\right) \quad (31)$$

$$H_{CO_2,\,H_2O}=\exp\left(145.369-\frac{8172.355}{T}-19.303\ln T\right) \quad (32)$$

Specifically, Henry's law constant of N_2O in MEA is calculated as follows:

$$H_{N_2O,\,MEA\text{-}sol}=H_{N_2O,\,H_2O}x_{H_2O}+H_{N_2O,\,MEA}x_{MEA}+3524641.533(x_{H_2O}x_{MEA})^2\left(1-\frac{T}{324.718}\right)\exp(-13.219x_{MEA}) \quad (33)$$

and then as follows:

$$H_{N_2O,\,MEA}=-9172.50+39.598T \quad (34)$$

where x_{H_2O} and x_{MEA} are the mole fraction of H_2O and MEA, respectively, in the solution.

2-6. Breakthrough Pressure

In a common HFMC process the liquid pressure was consistently maintained at a slightly higher level than the gas pressure to prevent the creation of bubbles. However, the liquid could penetrate into the membrane pores when the liquid pressure exceeded the breakthrough pressure. Consequently, the value associated with the breakthrough pressure is important information regarding the effective application of HFMC. In fact, from an application viewpoint, the probability of using a ceramic membrane for HFMC application at high pressure increased with increases in the breakthrough pressure. The breakthrough pressure (ΔP) could be calculated by Laplace-Young equation as follows [33]:

$$\Delta P=-\frac{2\gamma\cos\theta}{r_p} \quad (35)$$

where γ and θ denote surface tension and contact angle, respectively The surface tension (γ) was deducted from an extant study [34] and the contact angle is typically in the range from 100° to 120° [13].

RESULTS AND DISCUSSION

1. Comparison Between Experimental and Simulation Data

In the study, the model for the chemical absorption of CO_2 into the aqueous monoethanolamine (MEA) solutions from flue gases using porous alumina HFMC was verified by comparing the modeling results with the experimental data obtained in the lab-scale equipment. Specifically, the main parameters (i.e., a, b in Eq. (22)) derived from the model calibration were validated by experimental data for different gas velocities between 1.5×10^{-4} and 9×10^{-4} m/s. The parameter values were selected to minimize the objective function that was derived by comparing the simulation results and experimental data [35,36]. The objective function ($f_{objective}$) can be expressed as follows:

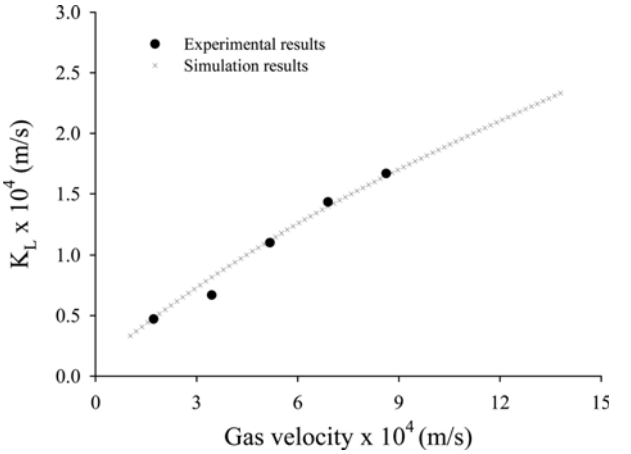

Fig. 2. Validation of the ceramic HFMC model by comparing simulation results and measured experiment data.

$$f_{objective}=\sum(\text{Exp}-\text{Sim})^2 \quad (36)$$

Fig. 2 presents the experimental results of the overall mass transfer coefficient (K_L) obtained as a function of gas velocity in the studied range (1.5×10^{-4}-9×10^{-4} m/s) and the simulation results obtained by the model examined in the present study. The corresponding values are given in Table 3. Evidently, as shown in Fig. 2, the simulated results were in good agreement with the experimental data. Note that the error between the modeling and experimental results calculated by the average absolute deviation (AAD) calculation method was estimated as approximately 2.86%. Specifically, AAD was determined from the experimental (Exp) and simulated (Sim) data for N data points by the following mathematical equation [37,38]:

$$AAD=\frac{1}{N}\sum\left|\frac{\text{Exp}-\text{Sim}}{\text{Exp}}\right|\times100\% \quad (37)$$

The a and b parameters in Eq. (22) were determined from the fitting curve equations reported in Fig. 2. This method indicated that the values of a and b parameters corresponded to 6.5 and 0.8, respectively. These results go beyond previous reports regarding polymeric HFMC, showing that the obtained values can be used to develop new models specifically for the ceramic HFMC case instead of that used in the polymeric membrane. It can be observed that there is a slight difference between previous values obtained in the polymeric HFMC cases (see Table 2) and the values estimated in the present study (see Table 3). This difference can be attributed to the characteristics of the ceramic membrane, low Reynolds number, and packing density. For example, the ceramic HFMC membranes are commonly manufactured with a large-scale diameter and thickness because most of the ceramic membranes are more frangible when compared with the polymeric membrane. Thus, the a and b parameters in the ceramic HFMC typically corre-

Table 3. Optimum parameters for the mass transfer of the ceramic HFMC

Parameter a	Parameter b	Reynolds number	Packing factor	AAD
6.5	0.8	0.0006<Re<0.003	Ø=0.004	2.86%

Table 4. Comparison of the CO_2 mass transfer coefficient for the HFMC

Experiment /model	Membrane material	Gas/flow rate	Liquid/flow rate	Overall mass transfer coefficient (m/s)	Reference
Experiment	Al_2O_3	15% CO_2/50 ml/min	20 wt% MEA/10 ml/min	1.67×10^{-4}	This work
	PVDF	20% CO_2/200 ml/min	6.1 wt% MEA/818.92 ml/min	7.43×10^{-7}	[39]
	Polytetrafluoroethylene (PTFE)	40% CO_2/170 ml/min	4 wt% AMP/111 ml/min	1.48×10^{-4}	[40]
	PP	20% CO_2/250 ml/min	3 wt% MEA/9 ml/min	5.0×10^{-4}	[41]
	PP	20% CO_2/200 ml/min	6.2 wt% MEA/17 ml/min	2.0×10^{-4}	[42]
	PP	14% CO_2/106 ml/min	18.6 wt% MEA/6.1 ml/min	5.6×10^{-4}	[43]
Model	Al_2O_3	15% CO_2/50 ml/min	20 wt% MEA/10 ml/min	1.65×10^{-4}	This work
	Hydrophobic polymer	Pure CO_2/30 ml/min	Pure water/60 ml/min	0.95×10^{-5}	[22]
	PTFE	15% CO_2/15 ml/min	18.3 wt% MEA/72 ml/min	5.00×10^{-4}	[31]
	PVDF	Pure CO_2/200 ml/min	12.2 wt% MEA/1045 ml/min	2.5×10^{-3}	[44]

sponded to large values when compared with those of the polymeric system. The ceramic HFMC model possessed an intrinsic value to also predict and verify the experimental results, and the model provided fundamental data for computer simulations and economic evaluations.

To the best of our knowledge, previous studies did not examine the HFMC or similar applications with other inorganic membranes. Therefore, it is difficult to systematically compare the information obtained in the present study regarding the porous alumina membranes with other kinds of organic membranes. Despite the fact that most studies have focused on the polymeric system, we attempted to compare our results with the results of the already published analysis on the polymeric HFMC with respect to experimental and modeling studies (see Table 4). As indicated by previous studies, the overall mass transfer coefficient (K_L) of the HFMC was approximately in the range of 7.43×10^{-7}-5.00×10^{-4} m/s even with variations in the operating conditions such as gas and liquid flow rates. The overall mass transfer coefficient obtained in this work is approximately 1.7×10^{-4} m/s, which corresponded to a very high level when compared with those obtained in previous studies on the polymeric HFMC. Hence, it was confirmed that alumina with high stability were alternatives for polymers with respect to membrane materials. Additionally, alumina HFMC possessed immense potential as a candidate for the CO_2 capture process subject to the optimization of the pore structure of the membrane and operating conditions (*i.e.*, liquid velocity and CO_2 concentration). In the next sections, these two aspects will be analyzed and compared to each other.

2. Effect of the Liquid Flow Rate and CO_2 Concentration on Mass Transfer

Fig. 3 shows the overall mass transfer coefficient relative to liquid flow rate (in the range of 0.3×10^{-3}-5×10^{-3} m/s) for three different CO_2 concentrations (5% CO_2, 15% CO_2, and 30% CO_2). The results indicate that the liquid velocity exerted a small effect on the mass transfer coefficient because the amount of liquid was sufficient to absorb the CO_2 and consequently the reaction rate between CO_2 and MEA increased. This fact was in good agreement with the data reported in previous studies for the MEA case [43,45,46]. In addition, it can be noted that the overall mass transfer coefficient increased based on the CO_2 concentration of the gas phase.

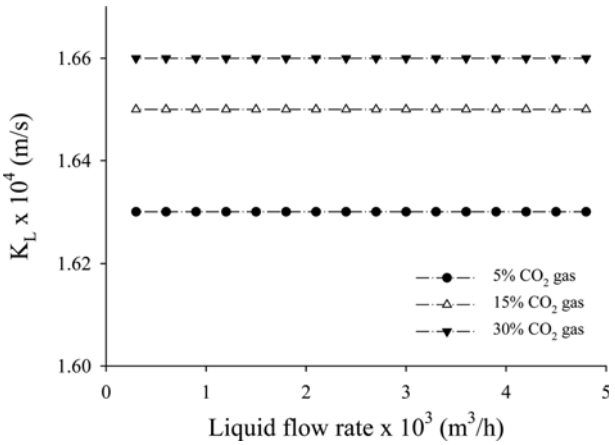

Fig. 3. The overall mass transfer coefficient based on liquid velocity and CO_2 concentration.

Specifically, the overall mass transfer coefficient increased from approximately 1.63 to 1.65×10^4 m/s (+1.2%) when the CO_2 concentration increased from 5% to 15%. This behavior can be attributed to the effect of an increase in driving force in accordance with an increase in the speed of gas diffusing into the liquid. In contrast, the effect of CO_2 concentration on the overall mass transfer coefficient did not double when the CO_2 concentration increased from 15% to 30%. The increased CO_2 concentration was only one of the different variables that caused the decrease in the gas phase mass transfer resistance based on Eq. (22). Additionally, the overall mass transfer resistance consisted of the liquid, membrane, and gas phase mass transfer resistances as shown in Eq. (2) and Fig. 4.

3. Liquid, Membrane and Gas Phase Mass Transfer Resistances

Fig. 4 shows the influence of the gas flow rate on the overall mass transfer resistance based on a resistance-in-series model approach. The overall mass transfer resistance decreased with increases in the gas flow rate. Specifically, the overall mass transfer resistance of the ceramic HFMC system decreased from 5608.8 s/m to 449.1 s/m when the gas flow rate increased from 0.005 m^3/h to 1 m^3/h. Furthermore, the three resistances (k_l, k_g and k_m) that acted in a series since they affected the overall rate of CO_2 transfer of the ceramic HFMC (see Fig. 1) were calculated from the validated model ob-

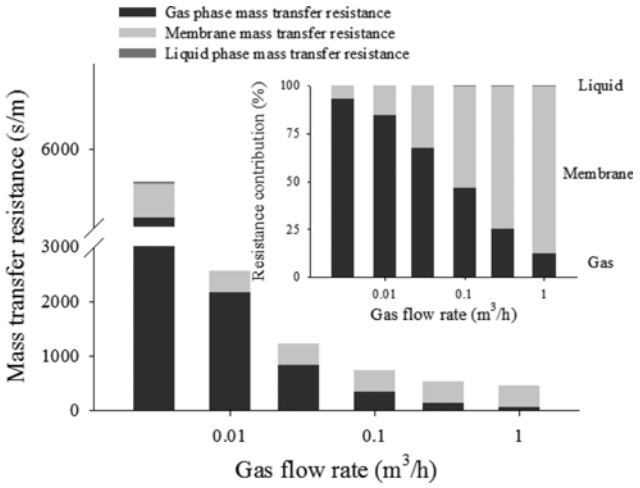

Fig. 4. Individual mass transfer resistance based on the gas flow rate.

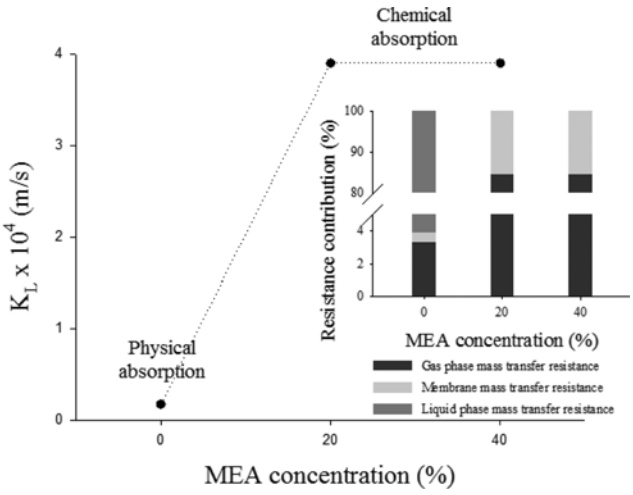

Fig. 5. The effect of MEA concentration on CO_2 mass transfer coefficient (composition of CO_2=15%, gas flow rate=0.01 m^3/h (=166.7 ml/min)).

tained in the previous section. The partial contributions of the three resistances on the overall mass transfer resistance (K_L) and based on the gas flow rate were separated in the study by Eq. (2) and equations were derived (as shown in Eq. (3)-Eq. (34)). Fig. 4 shows the histogram of the differences in value (s/m) and in percent (resistance contribution, %) of the mass transfer resistance contributions based on the gas flow rate.

Hence, the results indicated that the calculated liquid phase mass transfer resistance was very small and negligible in all the cases considered in the present study. For example, it is very interesting to note that the partial contribution of the liquid phase mass transfer resistance (k_l) constituted only approximately 0.43% of the overall mass transfer resistance when the gas flow rate corresponded to 1 m^3/h. Conversely, as shown in the Fig. 4, the value of the resistance associated with the gas phase (k_g) was dominant over the other resistances (i.e., liquid and membrane phase mass transfer resistances) with respect to the low gas flow rate. This fact is easily explained given that with respect to a low gas flow rate, sufficient gas could not be provided on the gas/membrane interface of a ceramic HFMC, and this could be responsible for the low liquid (k_l) and membrane (k_g) phase mass transfer resistance contributions. With respect to the membrane phase mass transfer resistance (k_m), this contribution predominated when the HFMC system was characterized by a high gas flow rate. From the results, it is clear that the structural optimization of the membrane phase nature is a key point for increasing the efficiency of the HFMC process by increasing the gas flow rate. In the next section, with the aim to extend our knowledge on advanced HFMC, the model will be extended to the structural characteristics of the membrane (i.e., membrane pore size and porosity).

According to the chemical reactions between the absorbate and the absorbent, it is well known that the absorption is divided into two parts: chemical absorption and physical absorption. This study mainly focused on the chemical absorption of CO_2 in aqueous MEA solution in a ceramic HFMC, but the properties of a pure physical absorption with only water (MEA 0%) were also investigated to explain the advantages of the chemical absorption. Fig. 5 shows the overall mass transfer coefficient as well as the each contribution of the gas phase, membrane and liquid phase mass transfer terms according to the MEA concentration between 0% and 40% MEA concentration. The overall mass transfer coefficient of the physical absorption was 22.5-times lower than that of the chemical absorption. In contrast to chemical absorption, physical absorption is a process dominated by the mass transfer resistance of the liquid phase (k_l) as shown in the right side of Fig. 5. That is because CO_2 could be hardly dissolved in water, whereas CO_2 was absorbed in MEA. Thus, liquid phase mass transfer is important part in physical absorption. From this point of view, it becomes evident why the chemical absorption with amine solution is commonly used for CO_2 capture to minimize the liquid phase mass transfer resistance and maximize the CO_2 absorption properties.

4. Membrane Optimization for Advanced HFMC Applications

4-1. Effect of the Membrane Pore Size and Porosity on Overall Mass Transfer Coefficient

Here we have investigated the effect of membrane structure on the HFMC performance by a numerical study of the overall mass

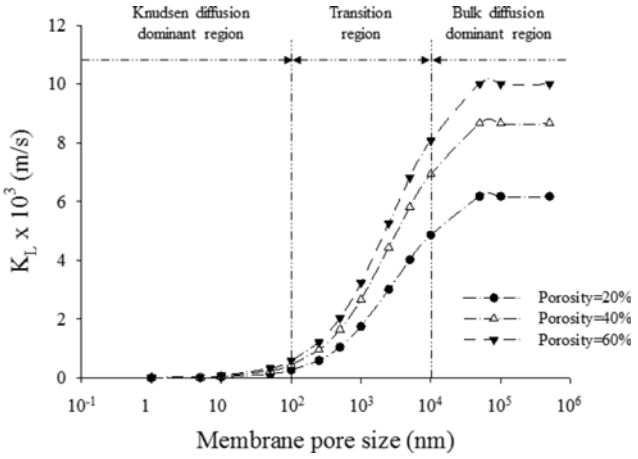

Fig. 6. Overall mass transfer coefficient based on the membrane pore size and porosity.

transfer coefficient. Fig. 6 shows the calculated overall mass transfer coefficient (m/s) relative to the membrane pore size (10^{-1}-10^{6} nm) for three different types of membrane porosities (20%, 40%, and 60%). The mean free path theory states that the gas diffusion mechanism is a function of membrane pore size and can be defined with Knudsen, bulk, and combined diffusion mechanisms [22]. Thus, the results indicate that the overall mass transfer coefficient is very low in the Knudsen diffusion dominant region (see the left side of Fig. 6) with extremely small membrane pore size. Hence, membranes with a small pore size (that is, a pore size less than 100 nm) are unsuitable for the ceramic HFMC system. In the transition region, the overall mass transfer coefficient increased with increases in the membrane pore size, and this implied that the collision between the CO_2 gas molecule and the pore walls decreased with increase in pore size in agreement with previous studies [8]. The overall mass transfer coefficient reached a maximum value in the bulk diffusion dominant region (see the right side of Fig. 6). Specifically, when the overall mass transfer coefficient reached a constant plateau, the value of saturation increased with increases in the porosity. At 60% of membrane porosity in the bulk diffusion dominant region (i.e., 10^5 nm<d_p), an overall mass transfer coefficient value of 10.02×10^{-3} m/s was observed. This indicated a 162% increase in the overall mass transfer coefficient with respect to an increase in membrane porosity from 20% to 60%. Hence, it can be concluded that the membranes should possess a high pore size (exceeding 10^5 nm) and high porosity to achieve high performance (i.e., overall mass transfer coefficient). As a result, with respect to these structural conditions (high membrane pore size and high porosity), the HFMC system worked as shown in the up-right side of the graph in Fig. 6.

4-2. Effect of the Membrane Pore Size on the Breakthrough Pressure

The breakthrough pressure is defined as the maximum pressure at which a liquid passes through the structure of a membrane and emerges from the opposite membrane surface. The breakthrough pressure is a very important variable affecting the applicability of HFMC. Also, membrane structural characteristics of the bulk as well as the nature of the ceramic membrane surface and, in particular, its hydrophobicity (i.e., contact angle) are all factors that affected the breakthrough pressure and then practical applications [47-50]. As is commonly known, hydrophobic modified porous alumina hollow fiber membrane displays a contact angle between 100° and 120° [13].

In this section, the analysis of the influence of the membrane pore size on the breakthrough pressure in a ceramic HFMC system characterized by different contact angles (100°, 110°, and 120°) was investigated.

As shown in Fig. 7, the breakthrough pressure increased with the increasing contact angle. However, from a practical viewpoint, it was very difficult to indefinitely increase the hydrophobicity due to the intrinsic nature of ceramic materials. Another interesting point is that it can be observed in Fig. 7 that the breakthrough pressure decreased with increases in the membrane pore size. A membrane in the bulk diffusion dominant region (see the right side of Fig. 7) exhibited almost zero breakthrough pressure (less than 0.15 bar) without any practical applications. Here, in apparent contrast with the discussion in the previous section, it can be assumed that

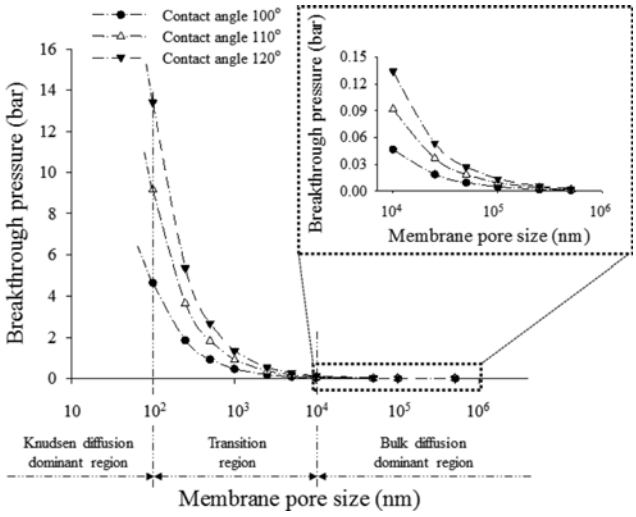

Fig. 7. Breakthrough pressure based on membrane pore size and contact angle.

high membrane stability (i.e., breakthrough pressure) for an HFMC process can be easily obtained with a membrane characterized by a low pore size distribution (i.e., less than 10^{-5} nm) and high hydrophobicity (i.e., contact angle). As a result, with respect to these structural conditions (i.e., low membrane pore size and high hydrophobicity), the HFMC system worked well as shown in the up-left side of the graph reported in Fig. 7.

This study examined the mathematical relationship between structural parameters (i.e., membrane pore size, porosity, and hydrophobicity) and the overall mass transfer coefficient and breakthrough pressure. Our results demonstrated that a ceramic membrane for advanced HFMC applications with an intermediate pore size between 10^2 nm and 10^4 nm, high porosity and high contact angle values, has all the characteristics specified for a good compromise between performance (overall mass transfer coefficient) and stability (breakthrough pressure).

CONCLUSION

Ceramic hollow fiber membrane contactors (HFMC) for CO_2 gas separation were examined experimentally and theoretically through absorption measurements of CO_2 in a monoethanolamine (MEA) solution and calculations. We derived the mass transfer coefficient (K_L) as a whole as well as its component parts - liquid phase mass transfer coefficient (k_l), membrane phase mass transfer coefficient (k_m), and gas phase mass transfer coefficient (k_g) - by applying a resistance-in-series model approach. There exists a considerable body of literature on polymer HFMC, but to our knowledge, this is the first report regarding the ceramic HFMC and the effects of the operating condition (i.e., gas and liquid flow rates, CO_2 and MEA concentrations) and membrane characteristics (i.e., membrane pore size, porosity, and hydrophobicity) on the overall mass transfer coefficient.

First, from the obtained results, it is clear that there is a good agreement between predicted and observed values with an average absolute deviation of 2.86%, indicating that the model was sig-

nificant. This is an important finding because it suggests that the applied model to the ceramic HFMC system has satisfactory predictive ability.

Second, the results of this study indicated that the membrane phase mass transfer resistance was more important than the other two resistances (liquid and gas phase mass transfer resistances) in a practical situation where the high gas flow rate is an important factor for large-scale industrial application. Thus, the study also verified that the ceramic HFMC membrane structure played a very import role in optimizing overall HFMC performance and applicability in the field of inorganic membranes.

Third, the same mathematical model was also used to examine the relationships between some specific structural parameters, such as membrane pore size and porosity, on the overall mass transfer coefficient. According to this model, the overall mass transfer coefficient of ceramic HFMC was found to be increased with increasing membrane pore size to a maximum value in the bulk diffusion dominant region with large pores (>10^4 nm). Also, as the porosity increased from 20% to 60%, the overall mass transfer coefficient of ceramic HFMC increased markedly.

In the last part of this study, mathematical correlations between pore size distributions, contact angle, and breakthrough pressure were investigated. The breakthrough pressure increased substantially with decreasing membrane pore size, reaching a maximum below 10^2 nm. At the same time, the breakthrough pressure increased with the contact angle from 100° and 120°, and this effect became more evident at low membrane pore sizes.

For practice, the results obtained in the present study showed that a compromise is needed between (1) performance achieved by designing a proper ceramic membrane with large pore sizes (>10^4 nm), on one side, and (2) applicability and stability thought a reasonable value of breakthrough pressure obtained by a membrane with small pores (<10^2 nm), on the other side. In conclusion, the broad implication of the present research is that optimal results were obtained using a ceramic HFMC with the membrane characterized by a pore size ranging from 10^2 nm to 10^4 nm. In this intermediate region, which was the result of a compromise, it can be seen that an appropriate increase in the membrane porosity and contact angle can effectively help to obtain higher overall mass transfer coefficient with a right breakthrough pressure.

ACKNOWLEDGEMENTS

This work was supported by a Korea CCS R&D Center (KCRC) grant funded by the Korean government (Ministry of Science, ICT & Future Planning) (No. 2014M1A8A1049314).

NOMENCLATURE

A : cross section area [m^2]
B : Boltzmann's constant
C_{CO_2}, $C^*_{CO_2}$: CO_2 concentration in solvent [mol/m^2]
$C_{CO_2,MEA}$: concentration of CO_2 in MEA solution [mol/m^3]
C_{MEA} : molarity of MEA solution [mol/m^3]
d_e : hydraulic diameter [m]
d_i, d_o, d_{lm} : hollow fiber outer, inner and log mean diameters [m]
d_p : membrane pore diameter [nm]
$D_{CO_2,gas}$: bulk diffusion coefficient [m^2/s]
D_{CO_2,H_2O} : diffusion coefficient of CO_2 in MEA solution [m^2/s]
$D_{CO_2,m}$: effective membrane diffusion coefficient [m^2/s]
$D_{CO_2,MEA}$: diffusion coefficient of CO_2 in the MEA solution [m^2/s]
D_{Kn} : Knudsen diffusion coefficient [m^2/s]
D_{MEA} : diffusion coefficient of MEA in aqueous MEA solution [m^2/s]
D_{N_2O,H_2O} : diffusion coefficient of N_2O in MEA solution [m^2/s]
$D_{N_2O,MEA}$: diffusion coefficient of N_2O in MEA solution [m^2/s]
E : enhancement factor
Exp : experimental data
E_∞ : infinite enhancement factor
Gz : Graetz number
H : Henry's law constant [$Pa \cdot m^3/mol$]
Ha : Hatta number
J_{CO_2} : mass transfer flux [$mol/m^2 \cdot s^{-1}$]
k : reaction rate constant of CO_2-MEA reaction [$m^3/mol \cdot s$]
k_g, k_m, k_l : mass transfer coefficient in gas, membrane, and liquid phase [m/s]
K_L : overall mass transfer coefficient [m/s]
M_{CO_2}, M_{N_2} : molecular weight of CO_2 and N_2
L : fiber length [m]
$p_{CO_2,g}$: partial pressure of the CO_2 in the gas phase [Pa]
P : pressure [Pa]
ΔP : breakthrough pressure [Pa]
r_p : membrane pore radius [m]
Re : Reynolds number
Sc : Schmidt number
Sh : Sherwood number
Sim : Simulated data
T : temperature [K]
T^* : dimensionless temperature
U : wetted perimeter [m]
v_l : liquid velocity [m/s]
v_R : stoichiometric coefficient
x_{H_2O}, x_{MEA} : mole fraction of H_2O and MEA in the solution
γ : surface tension
δ : membrane thickness [m]
ε : membrane porosity
ε_{CO_2}, ε_{N_2} : characteristic energy of CO_2 and N_2
θ : contact angle
μ : gas viscosity [kg/m·s]
ρ : gas density [kg/m^3]
σ_{CO_2}, σ_{N_2} : characteristic length of CO_2 and N_2 [Å]
τ_m : tortuosity
Ø : packing density
Ω_D : diffusion collision integral

REFERENCES

1. Y. Kim, J. Ryu and I. Lee, *Korean Chem. Eng. Res.*, **47**(5), 531 (2009).
2. G. Bakeri, M. Rezaei-DashtArzhandi, A. F. Ismail, T. Matsuura, M. S. Abdullah and N. B. Cheer, *Korean J. Chem. Eng.*, **34**(1), 160 (2017).
3. N. Nabian, A. A. Ghoreyshi, A. Rahimpour and M. Shakeri, *Korean J. Chem. Eng.*, **32**(11), 2204 (2015).

4. D. Jeong, M. Yun, J. Oh, I. Yum and Y. Lee, *Korean J. Chem. Eng.*, **27**(3), 939 (2010).
5. B. Ozturk and R. Hughes, *Chem. Eng. J.*, **195-196**, 122 (2012).
6. S. Boributh, W. Rongwong, S. Assabumrungrat, N. Laosiripojana and R. Jiraratananon, *J. Membr. Sci.*, **401-402**, 175 (2012).
7. S. A. Hashemifard, T. Matsuura, A. F. Ismail, M. R. D. Arzhandi, D. Rana and G. Bakeri, *Chem. Eng. J.*, **281**, 970 (2015).
8. K. Li, J. Kong and X. Tan, *Chem. Eng. Sci.*, **55**, 5579 (2000).
9. S. Atchariyawut, C. Feng, R. Wang, R. Jiraratananon and D. T. Liang, *J. Membr. Sci.*, **285**, 272 (2006).
10. G. Bakeri, A. F. Ismail, D. Rana and T. Matsuura, *Chem. Eng. J.*, **198-199**, 327 (2012).
11. F. Korminouri, M. Rahbari-Sisakht, T. Matsuura and A. F. Ismail, *Chem. Eng. J.*, **264**, 453 (2015).
12. L. Wang, Z. Zhang, B. Zhao, H. Zhang, X. Lu and Q. Yang, *Sep. Purif. Technol.*, **116**, 300 (2013).
13. H. J. Lee, E. Magnone and J. H. Park, *J. Membr. Sci.*, **494**, 143 (2015).
14. S. Koonaphapdeelert, Z. Wu and K. Li, *Chem. Eng. Sci.*, **64**, 1 (2009).
15. H. J. Lee and J. H. Park, *J. Membr. Sci.*, **518**, 79 (2016).
16. M. C. Yang and E. L. Cussler, *AIChE J.*, **32**, 1910 (1986).
17. H. Kreulen, C. A. Smolders, G. F. Versteeg and W. P. M. van Swaaij, *J. Membr. Sci.*, **78**, 197 (1993).
18. G. F. Versteeg and W. P. M. van Swaalj, *J. Chem. Eng. Data*, **33**, 29 (1988).
19. J. J. Ko, T. C. Tsai, C. Y. Lin, H. M. Wang and M. H. Li, *J. Chem. Eng. Data*, **46**, 160 (2000).
20. A. Gabelman and S.-T. Hwang, *J. Membr. Sci.*, **159**, 61 (1999).
21. J. L. Li and B. H. Chen, *Sep. Purif. Technol.*, **41**, 109 (2005).
22. S. Boributh, S. Assabumrungrat, N. Laosiripojana and R. Jiraratananon, *J. Membr. Sci.*, **380**, 21 (2011).
23. B. E. Poling, J. M. Prausnitz and J. P. O'connell, *Properties of gases and liquids*, fifth Ed., McGraw-Hill (2004).
24. M. C. Yang and E. L. Cussler, *AIChE J.*, **32**, 1910 (1986).
25. M. J. Costello, A. G. Fane, P. A. Hogan and R. W. Schofield, *J. Membr. Sci.*, **80**, 1 (1993).
26. P. Côté, J. L. Bersillon and A. Huyard, *J. Membr. Sci.*, **47**, 91 (1989).
27. R. Prasad and K. K. Sirkar, *AIChE J.*, **34**, 177 (1988).
28. W. J. DeCoursey, *Chem. Eng. Sci.*, **29**, 1867 (1974).
29. P. M. M. Blauwhoff, G. F. Versteef and W. P. M. van Swaaij, *Chem. Eng. Sci.*, **38**, 1411 (1983).
30. E. D. Snijder, M. J. M. te Riele, G. F. Versteeg and W. P. M. van Swaaij, *J. Chem. Eng. Data*, **38**, 475 (1993).
31. S. Khaisri, D. deMontigny, P. Tontiwachwuthikul and R. Jiraratananon, *J. Membr. Sci.*, **347**, 228 (2010).
32. A. Penttilä, C. Dell'Era, P. Uusi-Kyyny and V. Alopaeus, *Fluid Phase Equilib.*, **311**, 59 (2011).
33. V. Y. Dindore, D. W. F. Brilman, F. H. Geuzebroek and G. F. Versteeg, *Sep. Purif. Technol.*, **40**, 133 (2004).
34. S. A. Jayarathna, A. Weerasooriya, S. Dayarathna, D. A. Eimer and M. C. Melaaen, *J. Chem. Eng. Data*, **58**, 986 (2013).
35. M. Calderer, I. Jubany, R. Pérez, V. Martí and J. de Pablo, *Chem. Eng. J.*, **165**, 2 (2010).
36. J. H. Kim, S. K. Hong and S. J. Park, *Korean Chem. Eng. Res.*, **45**, 619 (2007).
37. E. Quijada-Maldonado, T. A. M. Aelmans, G. W. Meindersma and A. B. de Haan, *Chem. Eng. J.*, **223**, 287 (2013).
38. A. Aboudheir, P. Tontiwachwuthikul, A. Chakma and R. Idem, *Chem. Eng. Sci.*, **58**, 5195 (2003).
39. W. Rongwong, R. Jiraratananon, and S. Atchariyawut, *Sep. Purif. Technol.,* **69**, 118 (2009).
40. Y. Kim and S. Yang, *Sep. Purif. Technol.*, **21**, 101 (2000).
41. Y. Lv, X. Yu, S.-T. Tu, J. Yan and E. Dahlquist, *Appl. Energy*, **112**, 755 (2013).
42. Y. Lv, X. Yu, J. Jia, S.-T. Tu, J. Yan and E. Dahlquist, *Appl. Energy*, **90**(1), 167 (2012).
43. S. Yan, M. Fang, W. Zhang, S. Wang, Z. Xu, Z. Luo and K. Cen, *Fuel Process. Technol.*, **88**, 501 (2007).
44. W. Rongwong, S. Assabumrungrat and R. Jiraratananon, *J. Membr. Sci.*, **429**, 396 (2013).
45. S. Atchariyawut, R. Jiraratananon and R. Wang, *J. Membr. Sci.*, **304**, 163 (2007).
46. R. Faiz and M. Al-Marzouqi, *J. Membr. Sci.*, **342**, 269 (2009).
47. M. R. DashtArzhandi, A. F. Ismail, T. Matsuura, B. C. Ng and M. S. Abdullah, *Chem. Eng. J.*, **269**, 51 (2015).
48. M. Rahbari-Sisakht, D. Rana, T. Matsuura, D. Emadzadeh, M. Padaki and A. F. Ismail, *Chem. Eng. J.*, **246**, 306 (2014).
49. A. Hasanoğlu, J. Romero, B. Pérez and A. Plaza, *Chem. Eng. J.*, **160**, 530 (2010).
50. A. Mansourizadeh and A. F. Ismail, *Chem. Eng. J.*, **165**, 980 (2010).